Int. J. Heat Mass Transfer. Vol. 16, pp. 169–186. Pergamon Press 1973. Printed in Great Britain

THEORY OF THE ULTIMATE HEAT TRANSFER LIMIT OF CYLINDRICAL HEAT PIPES*

C. A. BUSSE
Euratom CCR, 21020 Ispra, Italy

(*Received* 22 *December* 1971 *and in revised form* 10 *April* 1972)

Abstract—The axial heat flux in heat pipes is limited in principle for two reasons: (1) insufficient return flow of condensate and (2) vapour flow limitations. If the liquid return flow is guaranteed by a suitable wick design, the axial heat flux is ultimately limited only by vapour flow effects. For this ultimate limit of heat transfer several vapour flow regimes can be distinguished depending on the relative magnitude of inertia- and viscous forces in the vapour.

An analysis of the ultimate limit of heat transfer of cylindrical heat pipes with laminar vapour flow is presented for the two limiting cases of either predominant inertia- or viscous forces (inertia and viscous flow regime), taking into consideration both the axial and radial variation of the vapour velocity. The radial variation of the axial velocity is decisive in the viscous flow regime, while in the inertia flow regime its influence turns out to be limited to a 5 per cent decrease of the ultimate limit of heat transfer. The vapour is described as an isothermal perfect gas. This model presents in the pressure ranges of analytical interest a fair approximation to reality (error in the heat transfer limits of about 10 per cent) and results in an especially simple analysis. In the inertia flow regime the heat flux is limited by the choking phenomenon (sonic heat transfer limit), while in the viscous flow regime the heat flux limitation stems from the fact that the vapour pressure cannot be smaller than zero (viscous heat transfer limit). Approximate formulae are derived for these two heat transfer limits. The analysis shows that for every heat pipe below a certain temperature the ultimate limit of heat transfer is of the viscous type. This limit can lie much below the sonic limit. Good agreement is found between theory and experimental data.

NOMENCLATURE

c_p, specific heat of the heat pipe vapour at constant pressure;
d, diameter of the vapour channel;
g, velocity profile correction;
h, specific enthalpy of the vapour;
h_{fg}, specific heat of vaporization of the working fluid;
l_a, l_c, l_h, length of heat shielded zone, cooling zone and heating zone;
l_{eff}, effective heat pipe length, defined by (13);
$\dot{q}$, axial heat flux density;
r, radial coordinate;
u, radial component of the vapour velocity;
v, absolute value of the vapour velocity;
v_s, sonic velocity;
w, axial component of the vapour velocity;
x, defined by (58);
z, axial coordinate;
A, defined as $\overline{w^2}/\overline{w}^2$;
M, average molar mass;
P, pressure;
R, universal gas constant = 1·987 cal/deg;
T, temperature;
T_b, boiling temperature;
T_{0t}, transition temperature between viscous and sonic heat transfer limitation;
η, viscosity of the vapour;
ξ, defined as $2\pi r^2/d^2$;
ρ, density of the vapour;
ρ_c, contribution of the condensate liquid to the vapour density;
Δ, absolute error.

Subscripts

l, condenser end of the heat pipe;

* Dedicated to Prof. Dr. F. Sauter for his 65th birthday.

m, maximum value in the heat pipe;
s, sonic limit;
t, transition from viscous to sonic heat transfer limitation;
v, viscous limit;
0, evaporator end of the heat pipe;
1, 2, monomer and dimer vapour species.

Superscripts

$\bar{}$, average over the cross section;
$'$, liquid vapour interface $r = d/2$;
$''$, heat pipe axis $r = 0$.

1. INTRODUCTION

A HEAT pipe (Fig. 1) consists of an evacuated container, the interior of which is lined with a wick, which is saturated with a working fluid. The heat is essentially transferred as latent energy by evaporating the working fluid in a

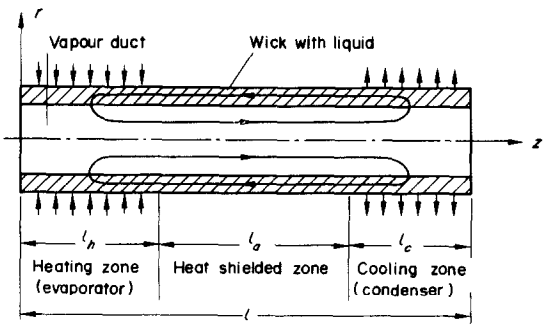

FIG. 1. Principle of the heat pipe and coordinate system.

heating zone and condensing the vapour in a cooling zone; the circulation is completed by the return flow of the condensate to the heating zone through the wick under the driving action of capillary forces [1].

The heat transport in heat pipes is limited by a number of effects, which can be divided into two groups. This is explained in Fig. 2, which is a schematical plot of the heat flux in a heat pipe versus the temperature drop between the two ends of the heat pipe. When no heat is transported, the temperature drop is zero and the

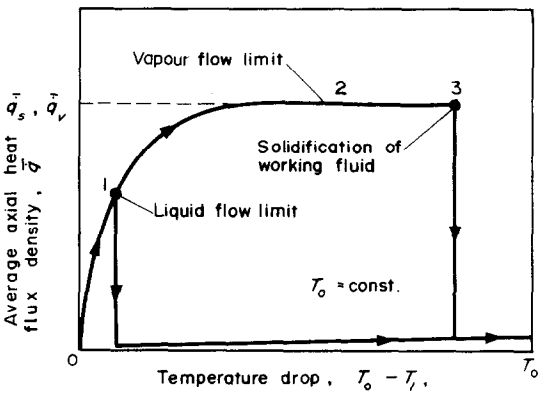

FIG. 2. Heat transfer limitations of a heat pipe (schematic).

heat pipe has a uniform temperature T_0. If one end of the heat pipe is cooled down to temperatures $T_l < T_0$ while the other end is kept at a constant temperature T_0, the heat flux increases very rapidly with $T_0 - T_l$.* Continuing this procedure to ever lower cooling zone temperatures one arrives at point 1, where the heat flux suddenly drops to nearly zero. This drop stems from an interruption of the circulation of the working fluid due to insufficient return flow of liquid, which can be caused by insufficient capillary pressure ("wicking limit") or by the formation of bubbles in the wick ("boiling limit"). Supposing that these liquid flow limitations can be overcome by suitable design of the wick, the heat flux would further increase with decreasing cooling zone temperature, then level off in a plateau 2 and finally drop to low values (point 3) when the cold end of the heat pipe reaches the melting temperature of the working fluid and the heat pipe is dried out by solidification of the working fluid at the cold end.

Plateau 2 is the subject of the following analysis. It stems from vapour flow limitations and presents an ultimate limit of the heat flux in the sense that it cannot be exceeded regardless

* The initial inclination of the curve, which is proportional to the effective thermal conductance of the heat pipe, can be several orders of magnitude larger than for a copper rod of the same size.

of wick construction. For these vapour flow limitations several regimes can be distinguished depending on the relative magnitude of inertia- and viscous forces in the vapour.

In the limiting case of negligible viscous forces ("inertia flow regime"), the vapour flow is limited by the well known choking phenomenon.* Choking occurs when the vapour pressure at the evaporator exit is as low as roughly half of the pressure at the upstream end of the evaporator. The axial heat flux then can no more be increased by a decrease of the pressure in the condenser (but only by an increase of the pressure and hence the temperature in the evaporator). In choked inertia flow the vapour leaves the evaporator with sonic speed. Therefore the related heat transfer limit is called the (inviscid) "sonic limit".

When both inertia and viscous forces play a role but the inertia forces predominate, the vapour flow is again limited by choking. In this case, however, choking occurs at the entrance of the condenser rather than at the exit of the evaporator. This means that the vapour still leaves the evaporator with subsonic speed, is expanded in the heat shielded zone to higher velocities and finally enters the condensor with sonic speed [8].

In the other limiting case of negligible inertia forces ("viscous flow regime") choking does not occur. The axial heat flux increases steadily with decreasing pressure at the evaporator exit and is finally limited by the fact that the vapour pressure cannot be smaller than zero. We shall call this the "viscous limit" of heat transfer.

In previous analytical work on the sonic limit of heat transfer four different vapour models have been used. This multiplicity stems from the fact that the vapour in the heating zone is formed in a nearly saturated condition and is subcooled in its expanding flow towards the cooling zone [2].† The four models differ in so far as supersaturation is concerned. In the first one, the "perfect gas model", the effects of supersaturation are neglected and the vapour is described as a perfect gas [3–6, 14]. In the second one, the "two-phase model", condensation is assumed to occur; the vapour is described as a mixture of a perfect gas and a liquid phase in equilibrium [4]. However, the formation of a liquid phase seems to be unlikely in view of two facts, first the lack of nucleation sites in the vapour duct and second the low degree of supersaturation [7]; the supersaturation is especially small for alkali metal vapours due to their very high heat capacity, which stems from association–dissociation reactions in these vapours (monomer $\rightleftarrows$ dimer). Therefore a third model has been used, the "association model", in which the vapour is described as a two-component mixture (monomer and dimer) of perfect gases, which is in local chemical equilibrium but which is "frozen" with respect to phase equilibrium, i.e. no condensation is assumed to occur [8]. Recently a fourth and more refined vapour model has been analyzed, in which the kinetics of the association–dissociation reaction and the droplet nucleation and growth process has been included [15]. Formulae for the sonic heat transfer limit have been derived only for the perfect gas model [3, 4, 6]. The other models have been evaluated by numerical analysis for some specific heat pipes [4, 8, 15]. It resulted that the sonic limit of heat transfer depends only slightly on the vapour model [4, 15] but that it can significantly be influenced by viscous effects [8, 15]. Except for [14], which presents a two dimensional numerical treatment of the perfect gas model, in all these studies on the sonic limit

* It results from the fact that an increase of the vapour velocity w by adiabatic expansion is coupled with a decrease of the vapour density ρ. Thus the increase of the mass flow density ρw by an increase of w is counteracted by the simultaneous decrease of ρ. If both effects are equally strong, the mass flow out of the evaporator can no more increased by a decrease of the pressure beyond the evaporator exit, i.e. choking occurs.

† It should be noted that supersaturation in general occurs in the inertia flow regime but not in the viscous flow regime where the heat produced by friction tends to keep the temperature of the gas constant along a stream line, similar as in a Joule–Thomson experiment (see appendix 1).

the vapour flow has been assumed as one-dimensional, that is the variation of the axial vapour velocity over the cross section of the vapour duct was neglected. So far no work on the limiting case of the viscous limit of heat transfer is known to have been done.

This paper gives an analytical treatment of vapour flow limitations in heat pipes both for limiting cases of inertia and viscous flow regime taking into consideration the axial and the radial variation of the vapour velocity. For this purpose the previously used vapour models are substituted by the uniform assumption of an isothermal dry vapour. This approach is suggested by the fact that for all previous vapour models the temperature variations as well as the liquid mass fraction (provided that condensation occurs) are relatively small in that pressure range, which is of importance for the evaluation of the vapour flow limits (see Appendix 1). The advantage of this isothermal dry vapour model is the uniformity of the analytical description and the simplicity of the analysis. The error in the calculated ultimate limits of heat transfer is estimated to be of the order of 10 per cent. This precision is sufficient for most practical purposes.*

2. BASIC EQUATIONS

The isothermal dry vapour is described by the equation of state of a perfect gas at constant temperature T_0, i.e.

$$\frac{P}{\rho} = \frac{P_0}{\rho_0} = \frac{RT_0}{M}. \tag{1}$$

The heat supplied to the heating zone is partly used for increasing the temperature of the liquid flowing in the wick and partly for evaporating it. That part of the heat, which is used for the temperature increase, is small against the evaporation part and can be neglected. Consistent with the isothermal approach the temperature dependence of the specific heat of vaporization h_{fg} is also neglected. Thus the net axial heat flow $(\dot{q} \cdot \pi d^2/4)$ becomes simply the product of the total mass of liquid, which evaporates per time unit, and the specific heat of vaporization h_{fg}. In the steady state this mass of evaporated liquid is equal to the mass of the vapour which flows out of the evaporator $(\overline{\rho w} \cdot \pi d^2/4)$. Therefore

$$\bar{\dot{q}} = \overline{\rho w} h_{fg}. \tag{2}$$

The radial variation of P,ρ and w and the axial pressure drop are derived from the Navier–Stokes equation of motion of the vapour assuming laminar vapour flow.* Using the equation of state (1) and assuming that the heat pipe is cylindrical, that the heat sources and sinks are distributed with axial symmetry around the vapour channel and that the heat pipe has a length which is large compared with the diameter, the Navier–Stokes equation can easily be solved by an approximation method similar to that of [9]. The three main results of this analysis, which is contained in Appendix 2, are the following ones:

(1) The radial variation of the pressure P is

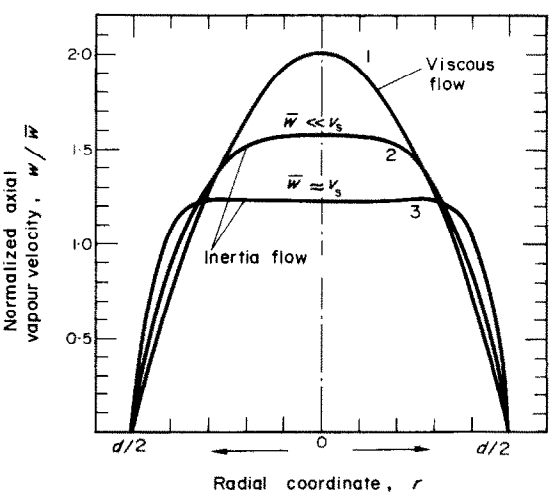

FIG. 3. Profiles of the axial vapour velocity.

* A suitable analytical method to obtain higher precisions would be to treat the temperature variations and the eventual liquid mass fraction as perturbations using the isothermal dry vapour model as zero order approximation.

* See introductory remarks of Appendix 3.

negligible and therefore also, because of (1), the radial variation of ρ, i.e.

$$\frac{\partial P}{\partial r} = \frac{\partial \rho}{\partial r} = 0. \tag{3}$$

(2) In the viscous flow regime the profile of the axial velocity is of parabolic shape ($w \sim 1 - 4r^2/d^2$), the same as in Poiseuille flow (Fig. 3, curve 1). In the inertia flow regime the velocity profile varies along the heat pipe. At the beginning of the heat pipe it is of the $\cos(2\pi r^2/d^2)$-type (Fig. 3, curve 2) known from incompressible flow analysis [9]. Along the heating zone the velocity profile becomes steadily flatter, reaching at the evaporator exit in the sonic limit a very flat shape (Fig. 3, curve 3).

(3) For the axial pressure drop the following equations hold: in the inertia flow regime (equation (48) of Appendix 2)

$$\bar{P}_0 - \bar{P}(z) = \overline{\rho(z) w^2(z)}\,, \tag{4a}$$

in the viscous flow regime (equation (42) of Appendix 2)

$$\frac{\mathrm{d}P}{\mathrm{d}z} = -\frac{32\eta}{d^2}\bar{w}(z). \tag{4b}$$

Equation (4a) is derived in Appendix 2 from the Navier–Stokes equation, but it can also be written down directly from the momentum balance. Equation (4b) is the same as for Poiseuille flow. The occurrence of $\overline{w^2}$ in equation (4a) necessitates in the following analysis the knowledge of the ratio $A \equiv \overline{w^2}/\bar{w}^2$. In Appendix 2 it is shown that A is a weakly variable function of the pressure ratio P_0/P (equations (55), (57) and (58)). This relationship is plotted in Fig. 4.

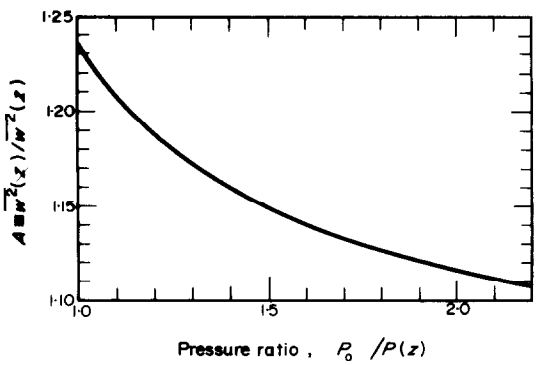

FIG. 4. Variations of $A \equiv \overline{w^2(z)}/\bar{w}^2(z)$ with pressure $P(z)$ in the inertia flow regime.

From equations (1)–(4) the heat transfer limits in the inertia and viscous vapour flow regimes can easily be determined.

3. SONIC HEAT TRANSFER LIMIT

Combining (1), (2) and (4a) and taking (3) into consideration it follows that

$$\bar{\dot{q}} = \frac{h_{fg}(\rho_0 P_0)^{\frac{1}{2}}}{A^{\frac{1}{2}}}\left[\frac{P}{P_0}\left(1 - \frac{P}{P_0}\right)\right]^{\frac{1}{2}} \tag{5}$$

This interesting equation permits to describe the pressure distribution along the heat pipe and is discussed in some detail in Appendix 3. For the moment we notice only that $\bar{\dot{q}}$ evidently has a maximum for a non-vanishing value of P, i.e. that choking of the vapour flow occurs. The condition for this maximum, which is the sonic limit of heat transfer, is obtained by putting $\mathrm{d}\bar{\dot{q}}/\mathrm{d}P = 0$. On finds that

$$\left(\frac{P}{P_0}\right)_s = \tfrac{1}{2}\left[1 + \left(\frac{P_0}{P} - 1\right)\frac{\mathrm{d}\ln A}{\mathrm{d}(P_0/P)}\right]_s. \tag{6}$$

Using the relationship between A and P_0/P, given by (56)–(58) or Fig. 4, equation (6) can readily be solved by iteration, yielding

$$\left(\frac{P_0}{P}\right)_s = 2{\cdot}08 \tag{7}$$

and

$$A_s = 1{\cdot}11. \tag{8}$$

With these two values it follows from (5) that the average axial heat flux density at the sonic limit of heat transfer

$$\boxed{\bar{\dot{q}}_s = 0{\cdot}474\, h_{fg}(\rho_0 P_0)^{\frac{1}{2}}.} \tag{9}$$

If the axial velocity of the vapour were assumed as constant over the cross section,

$A = \overline{w^2}/\bar{w}^2$ would be equal to one. Then, according to (6), the maximum of $\bar{\dot{q}}$ would occur at $P_0/P = 2$ and instead of the factor 0·474 in equation (9) a factor 0·5 would appear. This means that the radial variation of the axial vapour velocity causes a 5 per cent decrease of the sonic limit of heat transfer.

From (4a) one finds using (7) and (8) that at the sonic limit of heat transfer the average axial vapour velocity

$$\bar{w}_s = 0{\cdot}986(P_0/\rho_0)^{\frac{1}{2}}. \tag{10a}$$

Since for a gas with the equation of state (1) the velocity of sound $v_s = [\partial P/\partial\rho]^{\frac{1}{2}}_{\text{isentr.}}$ is equal to $(P_0/\rho_0)^{\frac{1}{2}}$, (10a) can also be written

$$\bar{w}_s = 0{\cdot}986\, v_s. \tag{10b}$$

This equation shows that the average axial vapour velocity at the sonic limit of heat transfer is in fact slightly below the sonic speed. This is due to the radial variation of the axial velocity; if namely the axial velocity is assumed to be constant over the cross section, i.e. $A = 1$ and $P_0/P = 2$, one finds instead of (10b) that $\bar{w}_s = v_s$.

Together with (10b) it follows from Fig. 3, curve 3, in agreement with [14] that at the sonic limit of heat transfer the vapour stream leaving the evaporator has a supersonic core (velocity on the axis some 20 per cent above sonic speed). This means that the transition to supersonic velocities begins already at some distance before the evaporator exit (roughly where $\bar{\dot{q}}$ reaches 80 per cent of the sonic limit).

4. VISCOUS HEAT TRANSFER LIMIT

Combining (1), (2) and (4b) and taking (3) into consideration it follows that

$$P\frac{\mathrm{d}P}{\mathrm{d}z} = -\frac{32\eta}{d^2}\frac{P_0}{h_{fg}\rho_0}\bar{\dot{q}}. \tag{11}$$

This equation shows that the pressure decreases steadily in down stream direction. Integrating along the heat pipe one finds that

$$P_0^2 - P_l^2 = \frac{64\eta}{d^2}\frac{P_0}{h_{fg}\rho_0}\int_0^l \bar{\dot{q}}(z)\mathrm{d}z. \tag{12}$$

Introducing the effective heat pipe length

$$l_{\text{eff}} = \frac{1}{\bar{\dot{q}}_m}\int_0^l \bar{\dot{q}}(z)\mathrm{d}z \tag{13}$$

which can be calculated from a knowledge of the relative distribution of heat sources and sinks on the heat pipe wall,* (12) can be resolved for maximum value of the average axial heat flux density in the heat pipe

$$\bar{\dot{q}}_m = \frac{d^2 h_{fg}}{64\eta l_{\text{eff}}}\left(1 - \frac{P_l^2}{P_0^2}\right)\rho_0 P_0. \tag{14}$$

$\bar{\dot{q}}_m$ increases with decreasing pressure at the end of the cooling zone and reaches a maximum, the viscous limit of heat transfer, when $P_l/P_0 = 0$†. Then

$$\boxed{\bar{\dot{q}}_v = \frac{d^2 h_{fg}}{64\eta l_{\text{eff}}}\rho_0 P_0.} \tag{15}$$

5. DISCUSSION

The temperature dependence of the viscous limit (15) and of the sonic limit (9) of heat transfer stems mainly from the factor $\rho_0 P_0$, which increases exponentially with temperature. While on the one hand the sonic limit is proportional to $(\rho_0 P_0)^{\frac{1}{2}}$, the viscous limit increases with $\rho_0 P_0$. Therefore at small values of $\rho_0 P_0$, i.e. of T_0, the heat flux will be limited by viscous effects, while for larger values of $\rho_0 P_0$, respectively T_0, the sonic limitation will dominate. The transition from one type of limitation to the other occurs in the temperature region where

* For example, if the heat input and output per surface area is constant along the heating and cooling zone, $\bar{\dot{q}}$ varies in these zones linearly with z and therefore $l_{\text{eff}} = \frac{1}{2}l_h + l_a + \frac{1}{2}l_c$.

† For the justification of the isothermal gas approach (see Appendix 1) it is important to note that the viscous limit is nearly reached already for rather large values of P_l/P_0. For example, if $P_l/P_0 = 0{\cdot}3$, $\bar{\dot{q}}_m = 0{\cdot}92\,\bar{\dot{q}}_v$.

the two heat flux limits (9) and (15) are of about the same magnitude. In order to get a criterion for the transition temperature T_{0t} one may equate the two heat fluxes (9) and (15), thus finding that

$$\left(\frac{l_{\text{eff}}}{d^2}\right)_t = 0{\cdot}033\left(\frac{(\rho_0 P_0)^{\frac{1}{2}}}{\eta}\right)_t. \qquad (16)$$

Using for ρ_0 and P_0 the values of saturated dry vapour, the right hand side of this equation can be expressed by the temperature T_{0t}. Figure 5 shows a plot of T_{0t} vs. l_{eff}/d^2 for Na, K and Cs.*

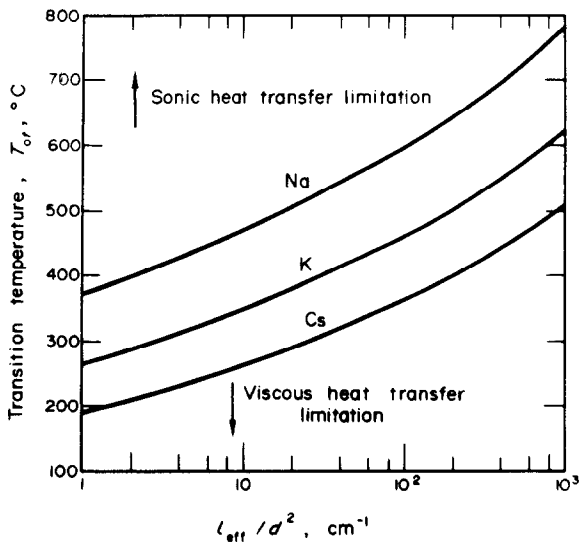

FIG. 5. Transition from viscous to sonic heat transfer limitation.

Thus a general conclusion is that for every heat pipe below a certain temperature T_{0t}, which depends on the working fluid utilized, the geometry of the heat pipe and the relative distribution of heat sources and sinks on the heat pipe wall, the ultimate heat transfer limit is of the viscous and not of the sonic type. This viscous limit can lie much below the sonic limit, a fact which e.g. needs attention in the analysis of heat pipe startup.

In Fig. 6 the theoretical heat transfer limits are compared with the experimental results of Kemme [5] obtained with Na, K and Cs heat

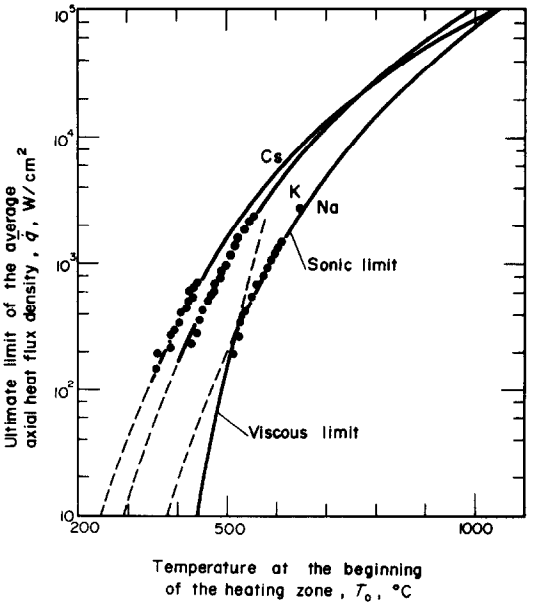

FIG. 6. Ultimate heat transfer limits (curves: theory; dots: experimental data of Kemme [5]).

pipes. The data points lie close to the sonic limit curves calculated from (9) except for the low temperature data of the Na and K heat pipes. For Na, where this deviation is most evident, the low temperature data fit well on the viscous limit curve (15) provided a transition temperature $T_{0t} = 525°C$ is assumed. With this value for T_{0t} it follows from Fig. 5 that $l_{\text{eff}}/d^2 = 32/\text{cm}$ and, since the heat pipe diameter was 1·14 cm, that $l_{\text{eff}} = 42$ cm. Kemme's paper does not allow a direct calculation of l_{eff} from the definition (13). However, the value of 42 cm seems to be well compatible with the dimensions of his Na heat pipe ($l_h = 14$ cm, $l_c = 110$ cm, $l_a \approx 5$–10 cm). Thus one may conclude that the

* For the calculation of Figs. 5 and 6 the η-values of [10] have been used; P_0 and ρ_0 were calculated from the thermochemical data of reference [11] taking into consideration both the monomer and dimer vapour component.

deviation of the low temperature Na-data from the sonic limit curve indicates the transition into the viscous flow regime.

If it is assumed that the effective length was the same for all three heat pipes (they were of nearly the same geometry, however the relative distribution of heat sources and sinks may have been different), one derives from Fig. 5 for the K- ($d = 1{\cdot}14$ cm) and Cs heat pipe ($d = 1{\cdot}11$ cm) transition temperatures of respectively 395°C and 310°C. Since all Cs data points stem from temperatures well above 310°C they sould fit on the sonic curve, which in fact is the case. Also for the K heat pipe the data points lie above the calculated transition temperature of 395°C, but they come relatively close to it. The deviation of the two lowest K data points from the sonic limit curve therefore could be either due to experimental scattering, or it could indicate that the transition temperature is in fact not 395°C but somewhat higher (about 430°C), which possibility cannot be excluded due to the uncertainty about the magnitude of the effective heat pipe length and the vapour viscosity.

With large temperature drops heat conduction along the pipe wall and liquid–wick matrix may not be negligible. In the foregoing examples an estimations shows that this conductive contribution should be of the order of only 1 W, which in fact is negligible compared with the total energy transport.

APPENDIX 1

Some thermodynamic considerations to compressible vapour flow in heat pipes

The sonic limit of heat transfer depends only on the evaporator section of the heat pipe, which according to (7) covers the pressure range

$$P_0 \geqslant P \gtrsim 0{\cdot}5\,P_0. \tag{17}$$

The viscous limit of heat transfer, on the other hand, depends on the entire length of the heat pipe and, strictly speaking, on the whole pressure range $P_0 \geqslant P \geqslant 0$. However, the pressure range of main importance for the analysis is

$$P_0 \geqslant P \gtrsim 0{\cdot}3\,P_0 \tag{18}$$

(see footnote to equation (15)). For these pressure ranges of analytical interest this appendix gives an evaluation of the maximum temperature variation and of the maximum possible mass fraction of condensate liquid in the vapour.

Let us consider first the liquid–vapour interface (see Fig. 7). There the vapour is assumed to

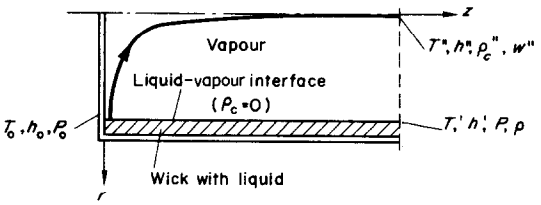

FIG. 7. Terms appearing in the evaluation of temperature variations and liquid mass fraction in the vapour.

be dry (i.e. $\rho_c = 0$) and saturated. This means that the temperature variations can be obtained from the given pressure variations (17) and (18) by the use of the Claussius–Clapeyron equation. For a perfect gas, neglecting the liquid volume,

$$\frac{\mathrm{d}T}{T^2} = \frac{R}{Mh_{fg}}\frac{\mathrm{d}P}{P}\,. \tag{19}$$

This equation holds also if the vapour (as in the case of alkali metals) is described as a mixture of two reacting perfect gases. Then,

$$P = P_1 + P_2 \tag{20a}$$

$$M = (P_1M_1 + P_2M_2)/P \tag{20b}$$

$$h_{fg} = (P_1M_1h_{fg1} + P_2M_2h_{fg2})/MP. \tag{20c}$$

Calculations from thermochemical data show that the molar heat of vaporization Mh_{fg} depends only little on temperature (less than M and h_{fg} itself). Therefore (19) may be integrated considering Mh_{fg} as constant. Thus one finds

for the relative temperature variation along the liquid–vapour interface

$$\frac{T_0 - T'}{T_0} = \frac{RT_0}{Mh_{fg}}\left(\ln\frac{P_0}{P}\right)\left[1 + \frac{RT_0}{Mh_{fg}}\ln\frac{P_0}{P}\right]^{-1}. \tag{21}$$

The temperature variations inside the vapour as well as the liquid mass fraction can be derived from the variation of the specific enthalpy. If non-convective heat transfer is neglected, conservation of energy requires that along any stream line $h + v^2/2$ is constant. The largest variation of the enthalpy occurs along the center stream line (Fig. 7) where

$$h_0 - h'' = \tfrac{1}{2}(w^2)''. \tag{22}$$

At the sonic limit, according to Fig. 3 and equations (10) and (1),

$$(w^2)'' \approx 1{\cdot}4v_s^2 = 1{\cdot}4\frac{RT_0}{M} \tag{23a}$$

while in the viscous flow regime

$$(w^2)'' \ll v_s^2 = \frac{RT_0}{M}. \tag{23b}$$

In order to evaluate from (22) the radial temperature differences and the liquid mass fraction in the vapour, the enthalpy difference $h_0 - h''$ is split up in an axial and a radial part (Fig. 7):

$$h_0 - h'' = (h_0 - h') + (h' - h''). \tag{24}$$

In radial direction P is constant. The radial enthalpy difference $h' - h''$ therefore depends on T and ρ_c only. In linear approximation

$$h' - h'' \approx \left(\frac{\partial h}{\partial T}\right)_{P,\rho_c=0}(T' - T'') - \left(\frac{\partial h}{\partial \rho_c}\right)_{P,T'}\rho_c'' = c_P(T' - T'') + h_{fg}\frac{\rho_c''}{\rho}. \tag{25}$$

Considering now the two extreme cases of no condensation and of maximum condensation (i.e. two-phase equilibrium) one finds the following results:

1. *No condensation.* Then

$$\rho_c = 0. \tag{26a}$$

Herewith it follows from (22)–(25) that

$$\frac{T'' - T'}{T_0} = \begin{cases} -\dfrac{0{\cdot}7 - M(h_0 - h')/RT_0}{Mc_P/R} & \text{(sonic limit)} \quad (26b) \\ \dfrac{h_0 - h'}{c_P T_0} & \text{(viscous limit)} \quad (26c) \end{cases}$$

2. *Maximum condensation.* Because of the two-phase equilibrium the radial constancy of P (39b) implies that also T is radially constant, i.e.

$$T'' - T' = 0. \tag{27a}$$

Herewith it follows from (22)–(25) that

$$\frac{\rho_c''}{\rho} = \begin{cases} \dfrac{0{\cdot}7 - M(h_0 - h')/RT_0}{Mh_{fg}/RT_0} & \text{(sonic limit)} \quad (27b) \\ -\dfrac{h_0 - h'}{h_{fg}} & \text{(viscous limit).} \quad (27c) \end{cases}$$

To evaluate equation (26) and (27), the axial enthalpy difference $h_0 - h'$ at the interface and the specific heat c_P of the saturated dry vapour at constant pressure have to be determined first. If the vapour is a perfect gas, the specific enthalpy depends on temperature only, i.e.

$$h_0 - h' = c_P(T_0 - T'). \tag{28a}$$

If furthermore the gas is monatomic, then in general

$$Mc_P = \tfrac{5}{2}R. \tag{28b}$$

If, on the other hand, the vapour is described as a two-component mixture (monomer and dimer) of perfect gases in chemical equilibrium, as in the case of alkali metals, the specific enthalpy of each vapour species is again a function of temperature only, but the enthalpy of the mixture

$$h = \frac{P_1M_1h_1 + P_2M_2h_2}{P_1M_1 + P_2M_2} \tag{29}$$

depends both on temperature and pressure. Since $M_2 = 2M_1$ and (for the cases considered

below) $P_2 \ll P_1$, equation (29) can be simplified to

$$h \approx h_1 + 2(h_2 - h_1)\frac{P_2}{P}. \quad (30)$$

For dry saturated vapour

$$h_2 - h_1 = h_{fg2} - h_{fg1}. \quad (31)$$

As this quantity depends only slightly on temperature, it follows from (30) that the axial enthalpy difference of the gas mixture along the interface

$$h_0 - h' \approx c_{p1}(T_0 - T') + 2(h_{fg2} - h_{fg1})\left(\frac{P_{20}}{P_0} - \frac{P_2}{P}\right). \quad (32a)$$

For the specific heat of the dry saturated gas mixture at constant pressure one finds from (29), using van't Hoff's relation for the temperature dependence of the equilibrium constant of a chemical reaction, that

$$c_p = \frac{P_1 c_{p1} + 2P_2 c_{p2}}{P_1 + 2P_2} + \frac{4P_1P_2(P_1 + P_2)}{(P_1 + 2P_2)^3}\frac{M_1}{RT^2}(h_{fg1} - h_{fg2})^2. \quad (32b)$$

The first term on the right hand side of this equation is the specific heat of the mixture if no reactions would occur between the two vapour species ("frozen" specific heat). The second term contains the contribution of the association-dissociation reactions. For $P_2 \ll P_1$ (32b) can be simplified to

$$c_p = c_{p1} + 4\frac{P_2}{P_1}\frac{M_1}{RT^2}(h_{fg1} - h_{fg2})^2. \quad (32c)$$

Table 1 shows the result of an evaluation of the foregoing equations for some alkali metal vapours at different temperatures using the thermochemical data from [11]. For comparison also a monatomic perfect gas has been included; in this case it was assumed, according to the rule of Pictet–Trouton, that $Mh_{fg} = 10RT_b$.

At the sonic limit of heat transfer the temperature drop $-(T' - T_0)/T_0$ along the liquid–vapour interface has values up to 6 per cent; values of this order of magnitude have in fact been observed [16]. In addition to that, if no condensation occurs in the vapour, a radial temperature drop towards the axis of the heat pipe exists indicating subcooling of the vapour. This radial temperature drop $-(T'' - T')/T_0$ is 22 per cent for the monatomic perfect gas and less than that for the alkali metal vapours (especially for Na), due to the dissociation–association reactions and the resulting high specific heat c_p.

Table 1. Temperature variations and liquid mass fraction in the pressure ranges of analytical interest

				Inertia flow regime (sonic limit) $P_0 \geqslant P \gtrsim 0{\cdot}5\,P_0$			Viscous flow regime $P_0 \geqslant P \gtrsim 0{\cdot}3\,P_0$	
	T_0 (°K)	$\frac{Mc_p}{R}$	$\frac{Mh_{fg}}{RT_0}$	$\frac{T' - T_0}{T_0}$ (%)	No condensation ($\rho_c = 0$) $\frac{T'' - T'}{T_0}$ (%)	Two-phase equilibrium ($T'' - T' = 0$) $\frac{\rho_c''}{\rho}$ (%)	$\frac{T' - T_0}{T_0}$ (%)	No condensation ($\rho_c = 0$) $\frac{T'' - T'}{T_0}$ (%)
Perfect gas (monatomic)	T_b	2·5	10	−6	−22	5	−11	11
Na	800	11·4	15·3	−4	−6	5	−7	≈0
	1000	11·1	12·2	−5	−7	6	−9	≈0
K	700	3·4	14·3	−5	−18	4	−8	5
	900	4·2	11·0	−6	−14	5	−10	4
Cs	600	4·3	14·4	−5	−14	4	−8	3
	800	5·3	10·6	−6	−12	6	−10	2

The maximum temperature variation, if no condensation occurs, is the sum of the axial- and the radial temperature drop and ranges between 28 per cent for the perfect monatomic gas and 10 per cent for Na at 800°K. If on the other hand, condensation occurs and a two-phase equilibrium exists, the mass fraction ρ_c''/ρ of condensate liquid in the vapour reaches values between 4 and 6 per cent. The radial temperature drop then is zero and the maximum temperature variation is equal to the axial temperature drop $-(T' - T_0)/T_0$ of 4–6 per cent.

At the viscous limit of heat transfer the temperature drop $-(T' - T_0)/T_0$ along the liquid–vapour interface is somewhat higher than at the sonic limit because of the larger pressure range of analytical interest. In radial direction there is in general a temperature increase towards the axis of the heat pipe, i.e. the vapour is not supersaturated. For the perfect gas this increase $(T'' - T')/T_0$ is as large as the axial drop along the interface, i.e. the temperature along the centre stream line of the heat pipe remains constant.* The physical mechanism behind this temperature constancy is the same as in a Joule–Thomson experiment: expansion energy is transformed by friction into heat, which keeps the vapour hot. Table 1 shows that for the alkali metal vapours the temperature increase $(T'' - T')/T_0$ towards the axis of the heat pipe is smaller than the axial drop $-(T' - T_0)/T_0$ along the liquid vapour interface, i.e. the temperature along the stream lines decreases. The reason for this is that with decreasing pressure a number of diatomic molecules dissociates; as this process for alkali metals is endothermic, heat is consumed, i.e. the vapour is cooled down. For Na this effect is so strong that the radial temperature difference in the heat pipe becomes roughly zero, i.e. the vapour in the heat pipe axis is just saturated. (Supersaturation by this dissociation effect is principally also quite possible.)

Summarizing one may say that the isothermal dry vapour model holds well when a two-phase equilibrium exists in the vapour. If there is no condensation the model is in the inertia flow regime a good approximation when c_p is large, i.e. when the association–dissociation reactions play an important role, while the approximation is relatively poor if the vapour behaves as a perfect gas. In the viscous flow regime the situation is just opposite.

The effect of the temperature variations and of ρ_c on $\bar{\dot{q}}$ can easily be estimated. From (2) and (4a) it follows that in the inertia flow regime for a given pressure essentially $\bar{\dot{q}} \sim \rho^{\frac{1}{2}}$. Similarly one obtains from (2) and (4b) that in the viscous flow regime $\bar{\dot{q}} \sim \rho$. Therefore at a constant pressure the relative errors of $\dot{q}$ and ρ are related as follows:

$$\frac{\Delta\bar{\dot{q}}}{\bar{\dot{q}}} \approx \begin{cases} \dfrac{\Delta\rho}{\rho} & \text{viscous flow} \\ \frac{1}{2}\dfrac{\Delta\rho}{\rho} & \text{inertia flow.} \end{cases}$$

The correct equation of state for the vapour is

$$\rho = \rho_c + \frac{MP}{RT}.$$

Therefore, for a given pressure,

$$\left|\frac{\Delta\rho}{\rho}\right| \lesssim \left|\frac{\rho_c}{\rho}\right| + \left|\frac{\Delta T}{T}\right|.$$

Herefrom it follows, taking the values of Table 1, that in the isothermal dry gas approximation the maximum relative errors of ρ for any pressure in the regions of analytical interest are respectively 28 per cent in the case of inertia flow and 11 per cent in the case of viscous flow. The resulting relative error $\Delta\bar{\dot{q}}/\bar{\dot{q}}$ is therefore at maximum roughly 14 and 11 per cent, respectively.

* This holds in fact for every stream line in the perfect gas, since in viscous flow according to (22) and (23b) h is constant along any stream line; as the enthalpy of a perfect gas depends on temperature only, this means that also T is constant along each stream line.

APPENDIX 2

Analysis of compressible laminar vapour flow in heat pipes

1. *Basic equations*

Laminar vapour flow is described by the Navier–Stokes equation (stationary case, no external forces)

$$\operatorname{grad} P = -\rho\left(\tfrac{1}{2}\operatorname{grad} v^2 - \boldsymbol{v}\times\operatorname{curl}\boldsymbol{v}\right) - \eta\left(\operatorname{curl}\operatorname{curl}\boldsymbol{v} - \frac{4}{3}\operatorname{grad}\operatorname{div}\boldsymbol{v}\right) \tag{33}$$

and the continuity equation

$$\operatorname{div}(\rho\boldsymbol{v}) \equiv \rho\operatorname{div}\boldsymbol{v} + \boldsymbol{v}.\operatorname{grad}\rho = 0. \tag{34}$$

In cylindrical coordinates for axial symmetry these equations can be written as follows:

$$\frac{\partial P}{\partial z} = -\rho\left(u\frac{\partial w}{\partial r} + w\frac{\partial w}{\partial z}\right) - \eta\left[\frac{1}{r}\frac{\partial}{\partial r}r\left(\frac{\partial u}{\partial z} - \frac{\partial w}{\partial r}\right) + \frac{4}{3}\frac{\partial}{\partial z}\operatorname{div}\boldsymbol{v}\right] \tag{35a}$$

$$\frac{\partial P}{\partial r} = -\rho\left(u\frac{\partial u}{\partial r} + w\frac{\partial u}{\partial z}\right) + \eta\left[\frac{\partial}{\partial z}\left(\frac{\partial u}{\partial z} - \frac{\partial w}{\partial r}\right) + \frac{4}{3}\frac{\partial}{\partial r}\operatorname{div}\boldsymbol{v}\right] \tag{35b}$$

$$\frac{1}{r}\frac{\partial}{\partial r}(r\rho u) + \frac{\partial}{\partial z}(\rho w) = 0 \tag{36}$$

with

$$\operatorname{div}\boldsymbol{v} = \frac{1}{r}\frac{\partial}{\partial r}(ru) + \frac{\partial w}{\partial z}. \tag{37}$$

The boundary conditions are

$$w = u = 0 \text{ on the end planes } z = 0 \text{ and } z = l \tag{38a}$$

$$w = 0 \qquad \text{on the liquid–vapour interface } r = \frac{d}{2}. \tag{38b}$$

If the length of each heat pipe zone (i.e. evaporator, heat shielded zone, condenser) is large against the diameter, u is in general small against w and therefore (35) can be simplified, similar as in Prandtl's boundary layer theory [12], to*

$$\frac{\partial P}{\partial z} = -\rho\left(u\frac{\partial w}{\partial r} + w\frac{\partial w}{\partial z}\right) + \frac{\eta}{r}\frac{\partial}{\partial r}r\frac{\partial w}{\partial r} \tag{39a}$$

$$\frac{\partial P}{\partial r} = 0. \tag{39b}$$

2. *Viscous flow regime*

In the viscous flow regime the inertia force term in (39a) is neglected. Because of (39b) P is a function of z only, i.e.

$$\frac{\mathrm{d}P}{\mathrm{d}z} = \frac{\eta}{r}\frac{\partial}{\partial r}r\frac{\partial w}{\partial r}. \tag{40}$$

Integrating twice over r one finds that

$$-\frac{1}{4}\frac{\mathrm{d}P}{\mathrm{d}z}\left(\frac{d^2}{4} - r^2\right) = \eta w. \tag{41}$$

By averaging over the cross section it follows that the axial pressure gradient

$$\frac{\mathrm{d}P}{\mathrm{d}z} = -\frac{32\eta}{\mathrm{d}^2}\bar{w}. \tag{42}$$

Herewith one obtains from (41) the profile of the axial velocity (Fig. 3, curve 1)

$$w = 2\bar{w}\left(1 - \frac{4r^2}{d^2}\right). \tag{43}$$

3. *Inertia flow regime*

Neglecting the viscous forces in (39a) it follows that

$$\frac{\partial P}{\partial z} = -\rho\left(u\frac{\partial w}{\partial r} + w\frac{\partial w}{\partial z}\right). \tag{44}$$

The radial velocity component u can be eliminated from this equation by means of the continuity equation (36). Integrating (36) over r from 0 to r and inserting it into (44) gives

* The validity of this approximation can also be verified *a posteriori* by inserting into (35) the velocity profiles calculated from (39).

$$\frac{\partial P}{\partial z} = \frac{\partial w}{\partial \xi}\frac{\partial}{\partial z}\int_0^{\xi} \rho w \mathrm{d}\xi - \rho w \frac{\partial w}{\partial z} \tag{45}$$

with

$$\xi = \frac{2\pi r^2}{d^2}. \tag{46}$$

In order to find an approximate solution of the system of equations (45) and (39b) a method similar to that of [9] will be used. For this purpose the average axial pressure drop and the axial pressure drop in the heat pipe axis are derived first.

By averaging equation (45) over the cross section one finds that on the right hand side the first term after partial integration can be combined with the second term (the integrated part vanishes because of the boundary condition (38)). It follows that

$$\frac{\mathrm{d}\bar{P}}{\mathrm{d}z} = -\frac{\mathrm{d}}{\mathrm{d}z}\overline{\rho w^2}. \tag{47}$$

By integration from $z = 0$ one finds with the boundary condition (38) that

$$\bar{P}_0 - \bar{P} = \overline{\rho w^2}. \tag{48}$$

(This equation can also directly be written down from the momentum balance.) Making use of the equation of state (1) in order to express ρ by P and taking into account the fact that because of (39b) P is radially constant one obtains

$$P_0 - P = \frac{\rho_0}{P_0} P\overline{w^2}. \tag{49}$$

On the heat pipe axis ($\xi = 0$) the first term of the right hand side of (45) vanishes. Eliminating ρ by means of (1) it follows that

$$\left(\frac{1}{P}\frac{\partial P}{\partial z}\right)'' = -\frac{\rho_0}{P_0}\left(w\frac{\partial w}{\partial z}\right)''. \tag{50}$$

Integrating this equation from $z = 0$ and taking into consideration (39b) it results with the boundary condition (38) that

$$\ln\frac{P_0}{P} = -\frac{\rho_0}{2P_0}(w^2)''. \tag{51}$$

For incompressible flow $\rho = \text{const.}$ the stable solution* of the system of equations (45 and (39b) under the boundary conditions (38) is given by

$$w = \frac{\pi}{2}\bar{w}(z)\cos\xi. \tag{52}$$

As one may expect that for compressible flow the profile of the axial velocity at the beginning of the heat pipe will be the same as for incompressible flow, the solution of (45) and (39b) is approximated by†

$$w(\xi, z) = \frac{\pi}{2}\bar{w}(z)\left[g_0(z) + g(z)\xi^2\right]\cos\xi. \tag{53}$$

g_0 can be expressed as a function of $g(z)$ by averaging (53) over the cross section. Thus one finds that

$$w = \frac{\pi}{2}\bar{w}(z)\left[1 + g(z)\left(\xi^2 + 2 - \frac{\pi^2}{4}\right)\right]\cos\xi. \tag{54}$$

The rigid solution of the equation (45) and (39b) is characterized by the fact that the pressure P is constant over the cross section. The approximation problem consists in determining the function $g(z)$ in (54) in such a way that P becomes as constant as possible over the cross section. The procedure is chosen so as to make the average deviation of P from a constant reference value equal to zero. As reference value the pressure in the axis of the heat pipe is chosen. This means that g is determined in such a way that $\bar{P} = P''$. For this purpose the ansatz (54) is inserted into equations (49) and (51), which

* There are still other solutions, which fulfil the boundary conditions (38) ($w \sim \cos[(2n + 1)\xi]$, $n = 1, 2, \ldots$). All these velocity profiles however are unstable since they have inflexion points (see e.g. [12]).

† One might consider to use a linear ξ-term instead of a square term. The velocity profile however turns out to be so flat it can be better approximated by a square-term (a linear ξ-term would lead to a pronounced minimum of the velocity profile in the axis).

are then resolved for g. Calculating at first from (54) $\overline{w^2}$ and $(w')^2$ one finds that

$$\frac{\overline{w^2}}{\bar{w}^2} \equiv A = \frac{\pi^2}{8}\left[1 - \left(\frac{\pi^2}{3} - 3\right)g + \left(\frac{\pi^4}{30} - \frac{2\pi^2}{3} + \frac{7}{2}\right)g^2\right] = 1{\cdot}234 - 0{\cdot}358g + 0{\cdot}206g^2 \quad (55)$$

and

$$\frac{(w')^2}{\bar{w}^2} = \frac{\pi^2}{4}\left[1 - \left(\frac{\pi^2}{4} - 2\right)g\right]^2 = 2{\cdot}468 - 2{\cdot}307\,g + 0{\cdot}539\,g^2. \quad (56)$$

Inserting this now into (49) and (51), eliminating $\bar{w}$ and resolving the resulting quadratic equation for g, one obtains

$$g = 2{\cdot}14\,\frac{x - 0{\cdot}310 - (1{\cdot}145\,x - 0{\cdot}669)^{\frac{1}{2}}}{x - 0{\cdot}765} \quad (57)$$

with

$$x \equiv \frac{\dfrac{P_0}{P} - 1}{\ln \dfrac{P_0}{P}}. \quad (58)$$

Figure 8 shows a plot of g vs. P_0/P calculated from equations (57) and (58). At the beginning of the evaporator $P_0/P = 1$ and $g = 0$. This means, as expected, that there the velocity profile (49) is the same as for incompressible flow ((52) and curve 2 in Fig. 3). With decreasing P, i.e. along the evaporator, g becomes larger and the velocity (54) flatter. At the sonic limit ($P_0/P = 2{\cdot}08$ (7)) g has a value of 0·47. The corresponding velocity profile is shown in Fig. 3, curve 3. The velocity profiles are similar to those derived in [14].

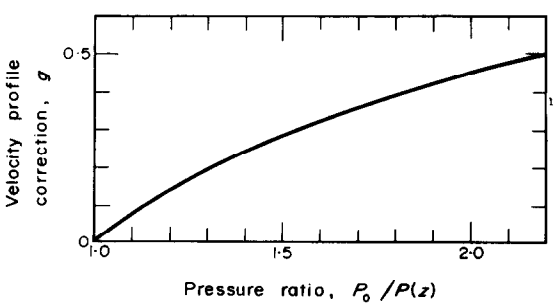

FIG. 8. Variation of the velocity profile correction with pressure (inertia flow regime).

The relation between $A \equiv \overline{w^2}/\bar{w}^2$ and P_0/P, which is required for the analysis of the sonic limit, is obtained from (55) with (57) and (58). Figure 4 is a graphical plot of this relation. The decrease of A with P reflects again the increasing flatness of the velocity profile.

APPENDIX 3

Pressure distribution along a heat pipe in the regime of compressible inertia flow

This appendix contains a discussion of equation (5), which relates the pressure P with the average axial heat flux density $\bar{q}$:

$$\bar{q} = \frac{h_{fg}(\rho_0 P_0)^{\frac{1}{2}}}{A^{\frac{1}{2}}}\left[\frac{P}{P_0}\left(1 - \frac{P}{P_0}\right)\right]^{\frac{1}{2}}. \quad (5)$$

If the relation between $\bar{q}$ and the axial coordinate z is known, this equation permits to obtain the pressure distribution along the heat pipe.

Before entering into the discussion attention has to be drawn to a limitation of equation (5). From incompressible vapour flow analysis in heat pipes [9] it is known that in the inertia flow regime the vapour, which enters the cooling zone, is relatively strongly slowed down near the wall and relatively little near the axis. As a result, at some distance from the condenser entrance, the velocity profile gets an inflexion point and somewhat later there is a region of reverse flow at the wall. This indicates that boundary layer separation will occur and that the vapour flow can no more be described by laminar analysis [12]. One may suspect that a similar effect occurs for compressible flow, i.e. that in the inertia flow regime only a relatively small part of the cooling zone can be described by a laminar theory. Thus equation (5), while it holds well in the heating zone, will probably

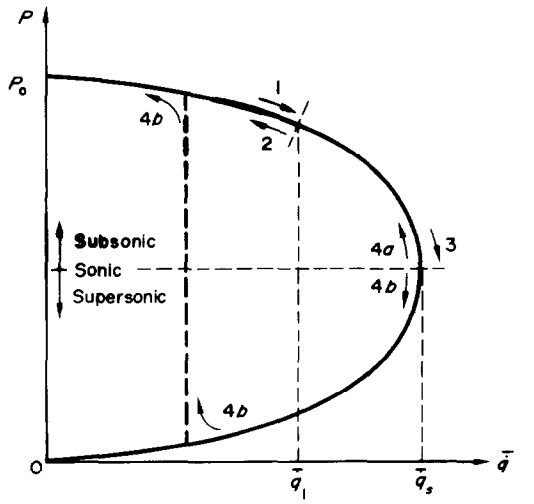

FIG. 9. Variation of pressure with average axial heat flux density in the inertia flow regime (schematic).

allow only qualitative conclusions in the cooling zone.

Figure 9 shows a plot of $\bar{q}$ vs. P from equation (5), taking $A = 1$ (then the sonic limit occurs at $P = 0{\cdot}5\,P_0$). Suppose that the heat pipe consists only of an evaporator and a condenser and that the radial heat input and output current

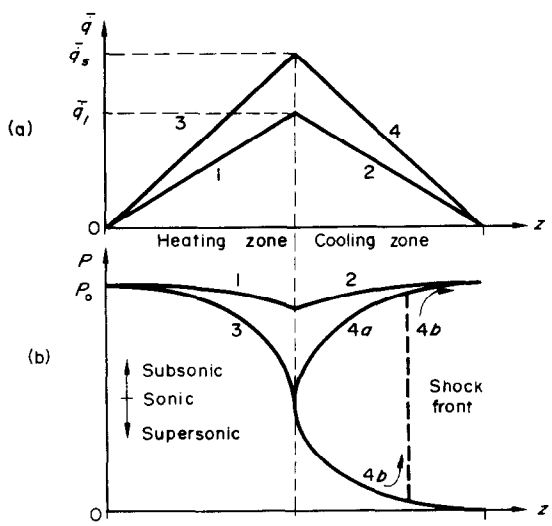

FIG. 10. Axial variation of average axial heat flux density and pressure (schematic).

densities are constant, i.e. that $\bar{q}$ varies linearly with z (Fig. 10a). Then the increase of $\bar{q}$ to a value $\bar{q}_1$ below the sonic limit of heat transfer and its subsequent decrease (curves 1 respectively 2 in Fig. 10a) correspond to a pressure decrease and increase in Fig. 9 as indicated by the flashes 1 and 2. The resulting axial pressure distribution is shown by the curve 1–2 in Fig. 10b. If the heat flux is increased up to the sonic limit (curve 3 in Fig. 10a), the pressure decreases as indicated by flash 3 in Fig. 9. For the decrease of the heat flux (curve 4 in Fig. 10b) there exist now two possibilities in the pressure diagram of Fig. 9: either an increase (flash 4a) or a decrease of pressure (flash 4b). Which path the system takes depends on the cooling system. It can easily be seen from (49) that the lower branch corresponds to supersonic vapour velocities. Equation (49) shows furthermore that this branch however cannot be followed down to $P = 0$ because of the boundary condition (38a), which requires that at the end of the cooling zone $P = P_0$. Therefore somewhere a compression shock has to occur in which the pressure jumps from the lower to the upper branch of Fig. 9. The corresponding axial pressure distributions are shown as curves 4a and 4b in Fig. 10b.

Because of the two-phase equilibrium, the temperature T is logarithmically linked with the pressure $P\,(1/T \sim \ln(1/P)$, see equation (19) of Appendix 1) and hence the curves of Fig. 10b give also an idea of the temperature distribution along the heat pipe. It is therefore interesting to compare Fig. 10b with experimental temperature distributions.

Figure 11 shows the temperature distributions along a heat pipe operated vertically in high vacuum. The heat pipe was 500 mm long. The lower part of 150 mm length was RF-heated, the rest was radiation cooled. The heat pipe was made of a smooth Nb–1Zr tube of 10 mm o.d. and 8 mm i.d. and a Nb–1Zr grid-type capillary insert [13] in the heating zone, which formed with the heat pipe wall 60 grooves of 0·1 mm width and 0·5 mm depth. The working fluid

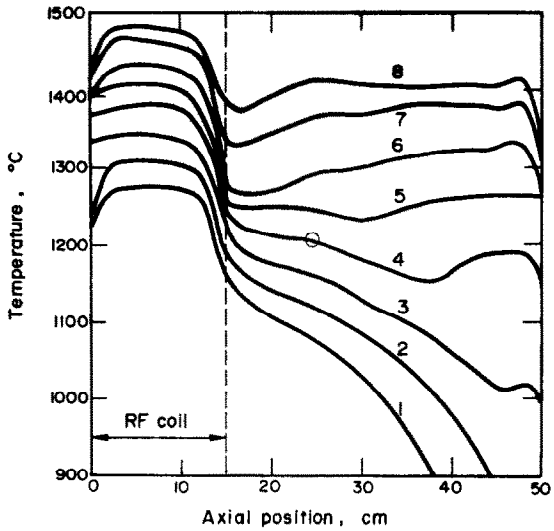

FIG. 11. Temperature distribution along a radiation cooled Nb-1Zr/Pb heat pipe of 10 mm o.d. and 500 mm length.

was Pb. The temperatures were measured by optical pyrometry at $z = 0,30,80$ and 130 mm, from $z = 150$ mm on at every 25 mm and towards the end of the cooling zone at every 12·5 mm.

It can be noted that curves 3, 4 and 5 in Fig. 11 have a temperature minimum in the cooling zone. This corresponds to the pressure curve 3–4b in Fig. 10b, i.e. left of the temperature minimum the flow should be supersonic and right of it subsonic; the minimum itself indicates the position of the shock front. Figure 11 shows that with increasing temperature the shock front moves towards the evaporator. Curve 6, where the shock front reaches the evaporator exit, corresponds then to the pressure curve 3–4a in Fig. 10b. For curves 7 and 8 of Fig. 11 the flow is everywhere subsonic, corresponding to the pressure curve 1–2 in Fig. 10b. The subsonic flow for curves 7 and 8 is also confirmed by the fact that from curve 6 to 8 a pronounced decrease of the temperature drop in the heating zone occurs, as one would expect from comparison of the pressure curves 3 and 1 in Fig. 10b.

Thus equation (5) explains qualitatively a number of the main features of Fig. 11. It does not explain the occurrence (or non-occurrence) of the temperature drops at the heat pipe ends shown in Fig. 11, which possibly are due to the accumulation of working fluid.

Quantitatively, however, there are essential differences between Fig. 10b and Fig. 11. Most evident is the fact that in Fig. 11 no complete pressure recovery occurs and that the shock front is not very sharp. These differences are probably mainly due to two effects: First, the heat pipe was not operated strictly in the inertia flow regime. An estimation shows that below roughly 1200°C the viscous forces may no longer be negligible. Second, in the inertia flow regime, i.e. above roughly 1200°C, the initially mentioned boundary layer separation occurs in the cooling zone so that the vapour flow is no longer completely laminar. This is also experimentally supported by the fact that on curve 4 of Fig. 11 at the position marked by a circle rapid temperature fluctuations were observed (they were found nowhere else). Finally it must be noted that the heat conduction in the heat pipe wall (Nb–1Zr is a rather good heat conductor) will also smooth out the wall temperature variation in the region of the shock front.

REFERENCES

1. G. M. GROVER, T. P. COTTER and G. F. ERICKSON, Structures of very high thermal conductance, *J. Appl. Phys.* **35**, 1990 (1964).
2. T. P. COTTER, Heat pipe startup dynamics, IEEE Conference Record of the Thermionic Conversion Specialist Conference, Palo Alto, p. 344 (1967).
3. E. VAN ANDEL, Heat pipe design theory, 2nd Int. Conf. Thermionic Electrical Power Generation, Stresa, EUR 2410 f.e., p. 529 (1968).
4. E. K. LEVY, Theoretical investigation of heat pipes operating at low vapour pressures, *Trans. Am. Soc. Mech. Engrs.* **90B**, 547 (1968).
5. J. E. KEMME, Ultimate heat pipe performance, *IEEE Trans. Electron Devices* **ED-16**, 717 (1969).
6. J. E. DEVERALL, J. E. KEMME and L. W. FLORSCHUETZ, Sonic limitations and startup problems of heat pipes, Los Alamos Scientific Laboratory, LA-4518 (1970).
7. G. S. DZAKOWIC, Discussion of paper entitled theoretical investigation of heat pipes operating at low vapor pressures, *J. Engng Ind.* **91**, 288 (1969).
8. E. K. LEVY, Effects of friction on the sonic velocity limit in sodium heat pipes, AIAA 6th Thermophysics Conference, April 26–28 (1971).

9. C. A. BUSSE, Pressure drop in the vapor phase of long heat pipes, 1967 IEEE Conference Record of the Thermionic Conversion Specialist Conference, Palo Alto, p. 391 (1967).
10. W. D. WEATHERFORD, JR., J. C. TYLER and P. M. KU, Properties of inorganic energy-conversion and heat-transfer fluids for space applications, WADD TR 61–96 (1961).
11. D. R. STULL *et al.*, *JANAF Thermochemical Tables*, PB 168 370 (1965) and third addendum PB 168 370–3 (1968).
12. H. SCHLICHTING, *Grenzschicht Theorie*, 5th edition. Verlag G. Braun, Karlsruhe (1965).
13. C. A. BUSSE, R. CARON, F. GEIGER and M. PÖTZSCHKE, Performance studies on heat pipes, Int. Conf. on Thermionic Electrical Power Generation, London, Institution of Electrical Engineers (1965).
14. D. DEMICHELE, A numerical solution to axial symmetric compressible flow with mass injection and its application to heat pipes, Pd.D. thesis, Department of Nuclear Engineering, University of Arizona (1970).
15. E. K. LEVY and S. F. CHOU, Sonic limit in sodium heat pipes, ASME paper 71-WA/HT-11(1971).
16. G. DZAKOWIC, T. TANG and F. ARCELLA, Experimental study of vapor velocity limit in a sodium heat pipe, ASME paper 69-HT-21 (1969).

THEORIE DE LA LIMITE ULTIME DE TRANSFERT THERMIQUE POUR DES CALODUCS CYLINDRIQUES

Résumé—Le flux thermique axial dans des caloducs est en principe limité pour deux raisons: l'insuffisance de l'écoulement de retour du condensat et les limitations de l'écoulement de vapeur. Si l'écoulement liquide de retour est garanti par une mèche convenable, le flux thermique axial est limité par les seuls effets de l'écoulement de vapeur. Pour cette limite ultime du transfert thermique, on a pu distinguer plusiers régimes d'écoulement de vapeur dépendant de la grandeur relative des forces d'inertie et de viscosité dans la vapeur.

On présente pour les deux cas limites de la prédominance soit des forces d'inertie soit des forces de viscosité (régime d'écoulement inertiel ou visqueux), une analyse de la limite ultime du transfert thermique dans des caloducs cylindriques en considérant à la fois les variations axiales et radiales de la vitesse de la vapeur. La variation radiale de la composante axiale de la vitesse est décisive dans le régime d'écoulement visqueux tandis que dans le régime d'écoulement inertiel son influence est réduite à une diminution de 5 pour cent pour la limite ultime du transfert thermique. La vapeur est décrite comme un gaz parfait isotherme. Ce modèle présente dans les domaines de pression intéressants une approximation convenable de la réalité (erreur sur les limites du transfert thermique de l'ordre de 10 pour cent) et il repose sur une analyse particulièrement simple. Dans le régime d'écoulement inertiel, le flux thermique est limité par le phénomène de choc (limite de transfert thermique sonique), tandis que dans le régime d'écoulement visqueux la limitation du flux thermique résulte du fait que la pression de vapeur ne peut être inférieure à zéro (limite de transfert thermique visqueux). On obtient des formules approchées pour ces deux limites de transfert thermique. L'analyse montre que pour chaque caloduc, au dessous d'une certaine température, la limite ultime du transfert thermique est du type visqueux. Cette limite peut être très inférieure à la limite sonique. Un bon accord existe entre les résultats théoriques et expérimentaux.

DIE THEORIE DER ENDGÜLTIGEN WÄRMEÜBERTRAGUNGSGRENZE ZYLINDRISCHER WÄRMEROHRE

Zusammenfassung – Der axiale Wärmestrom in Wärmerohren wird im Prinzip aus zwei Ursachen begrenzt: unzureichender Rückfluss des Kondensats und Dampfströmungsbegrenzungen. Falls der Flüssigkeitsrückstrom durch eine geeignete Dochtgestaltung garantiert ist, wird der axiale Wärmestrom nur noch durch Dampfströmungseffekte begrenzt. Für diese endgültige Grenze der Wärmeübertragung kann man verschiedene Strömungsbereiche unterscheiden, abhängend von der relativen Grösse der Trägheits- und Zähigkeitskräfte im Dampf.

Eine Analyse der endgültigen Grenze der Wärmeübertragung zylindrischer Wärmerohre mit laminarer Dampfströmung wird für die zwei begrenzenden Fälle, entweder Überwiegend Trägheits- oder Zähigkeitskräfte (Trägheits- oder zäher Strömungsbereich) vorgelegt, unter Berücksichtigung sowohl der axialen als auch der radialen Änderung der Dampfgeschwindigkeit. Die radiale Änderung der Axialgeschwindigkeit ist entscheidend im viskosen Strömungsbereich, während sich im Trägheits-Strömungsbereich ihr Einfluss als begrenzt erweist mit einer Verminderung der endgültigen Grenze der Wärmeübertragung um 5 Prozent. Der Dampf wird als isothermes, ideales Gas angesehen. Dieses Modell gibt in dem analytisch interessierenden Druckbereich eine recht gute Näherung zur Wirklichkeit (Fehler in den Wärmeübertragungsgrenzen von ungefähr 10 Prozent) und liefert Ergebnisse durch eine besonders einfache Analyse. Im Trägheits-Strömungsbereich wird der Wärmestrom durch das Drossel-Phänomen begrenzt (Schallströmungs-Wärmeübertragungsgrenze), während im viskosen Strömungsbereich die Wärmestrombegrenzung daher

rührt, dass der Dampfdruck nicht kleiner als Null sein kann (viskose Wärmeübertragungsgrenze). Die Näherungsformeln wurden für diese zwei Wärmeübertragungsgrenzen abgeleitet. Die Untersuchung zeigt, dass für jedes Wärmerohr unterhalb einer bestimmten Temperatur die grundlegende Grenze der Wärmeübertragung vom viskosen Typ ist. Diese Grenze kann weit unterhalb der Schallgrenze liegen. Zwischen der Theorie und den experimentellen Ergebnissen wurde eine gute Übereinstimmung gefunden.

ТЕОРИЯ ПРЕДЕЛА ВОЗМОЖНОСТЕЙ ТЕПЛОПЕРЕНОСА В ЦИЛИНДРИЧЕСКИХ ТЕПЛОВЫХ ТРУБКАХ

Аннотация—Имеются два принципиальных ограничения переноса тепла в осевом направлении тепловых трубок: недостаточный возврат конденсата и ограничения по потоку пара. Если возврат жидкости достигается соответствующей конструкцией фитиля, то теплоперенос в конечном счете ограничивается только воздействием потока пара. Поэтому предел возможностей теплопереноса при разных режимах течения пара может быть различным в зависимости от относительной величины сил инерции или вязкости в потоке.

Выполнен анализ предела возможностей передачи тепла в цилиндрических тепловых трубках при ламинарном течении пара для двух предельных случаев (инерционного и вязкого течений) с учетом как осевой, так и радиальной составляющих скорости пара. Изменение осевой скорости по радиусу является определяющим при вязком течении, тогда как при инерционном течении ее влияние сказывается в уменьшении на 5% возможностей теплопереноса. Пар рассматривается как изотермический идеальный газ. Такая модель проста и имеет хорошее соответствие с реальным процессом для интервала давлений, представляющих теоретический интерес (погрешность предела возможностей составляет около 10%). При инерционом течении тепловой поток ограничивается вследствие ударных явлений (звуковой предел), в то время как при вязком тчении ограничения теплового потока обусловлены тем, что давление пара не может быть меньше нуля (вязкий предел). Получены аппроксимирующие зависимости для этих двух предельных случаев теплообмена. Анализ показывает, что для каждой тепловой трубки ниже некоторой температуры конечный предел возможностей теплообмена определяет предел, который может быть намного ниже звукового. Обнаружено хорошее соответствие между теоретическими и экспериментальными данными.